Hemispherical Backscattering by Aerosols

PETR CHÝLEK

Department of Atmospheric Science, State University of New York, Albany 12222

G. W. GRAMS AND G. A. SMITH

National Center for Atmospheric Research,[1] Boulder, Colo. 80303

P. B. RUSSELL

Stanford Research Institute, Menlo Park, Calif. 94025

(Manuscript received 12 April 1974, in revised form 2 December 1974)

ABSTRACT

Hemispherical backscattering cross sections σ_b of spherical particles are calculated using a recently derived analytic expression. Results are compared with σ_b values obtained by numerical integration. It is found that the analytic formula gives exact values of the hemispherical backscattering cross sections and also saves computer time. The behavior of σ_b in the limits of very small and very large spheres is discussed. As an aid in utilizing simple models of climate change due to aerosols, the percentage of incident solar radiation scattered into the backward hemisphere is calculated for a range of particle sizes and complex refractive indices. Similar results are also presented for the ratio of absorption to hemispheric backscattering, a critical parameter in many aerosol climate models.

1. Introduction

Recently, considerable attention has been devoted to the possible effects of atmospheric aerosols on the global climate. In many of these studies (Atwater, 1970; Mitchell, 1971; Ensor *et al.*, 1971; Chýlek and Coakley, 1974) some kind of analytic condition relating the earth-atmosphere albedo, aerosol absorption, and aerosol scattering into the backward hemisphere is derived. This relation, usually called the heating condition, determines whether an additional aerosol layer will heat or cool the earth-atmosphere system. Therefore, numerical calculations in these studies involve the evaluation of the aerosol hemispherical backscattering cross section σ_b. Assuming that the aerosol particles are spherical, we can use the formalism of Mie scattering wherein σ_b is given by

$$\sigma_b=\frac{\lambda^2}{2\pi}\int_{-1}^{0}[|S_1(\theta,x,m)|^2+|S_2(\theta,x,m)|^2]d\mu, \quad (1)$$

where θ is the scattering angle, $m=n-n'i$ is the complex index of refraction of an aerosol particle, $x=2\pi r/\lambda$ is a size parameter relating the radius of the sphere r to the wavelength λ of the incident electromagnetic wave, and $\mu=\cos\theta$. The scattering amplitudes S_1 and S_2 are given by

$$S_1(\theta,x,m)=\sum_{k=1}^{\infty}\frac{2k+1}{k(k+1)}[a_k(x,m)\pi_k(\theta)+b_k(x,m)\tau_k(\theta)], \quad (2a)$$

$$S_2(\theta,x,m)=\sum_{k=1}^{\infty}\frac{2k+1}{k(k+1)}[a_k(x,m)\tau_k(\theta)+b_k(x,m)\pi_k(\theta)]. \quad (2b)$$

The Mie scattering functions a_k and b_k can be written as

$$a_k(x,m)=\frac{\psi_k(x)\psi_k'(mx)-m\psi_k(mx)\psi_k'(x)}{\zeta_k(x)\psi_k'(mx)-m\psi_k(mx)\zeta_k'(x)}, \quad (3a)$$

$$b_k(x,m)=\frac{m\psi_n(x)\psi_n'(mx)-\psi_n(mx)\psi_n'(x)}{m\zeta_n(x)\psi_n'(mx)-\psi_n(mx)\zeta_n'(x)}, \quad (3b)$$

where ψ_k and ζ_k are the Riccati-Bessel functions and ψ_k' and ζ_k' are their derivatives with respect to the arguments.

Finally, the angular function $\pi_k(\mu)$ and $\tau_k(\mu)$ are

[1] The National Center for Atmospheric Research is sponsored by the National Science Foundation.

determined by

$$\pi_k(\mu)=\frac{dP_k(\mu)}{d\mu}, \tag{4a}$$

$$\tau_k(\mu)=\mu\pi_k(\mu)-(1-\mu^2)\frac{d\pi_k(\mu)}{d\mu}, \tag{4b}$$

where P_k are Legendre polynomials.

Consequently, the integrand in (1) is a rather complicated expression and the integration has heretofore been done numerically. Recently it was shown that the integration in (1) can be evaluated analytically, and a formula for Mie scattering into the backward hemisphere was derived (Chýlek, 1973). The hemispherical backscattering cross section is given by

$$\sigma_b=\frac{\lambda^2}{4\pi}\Big[\sum_{k=1}^{\infty}(2k+1)(|a_k|^2+|b_k|^2)+2\sum_{k=2}^{\infty}{}''\sum_{l=1}^{\infty}{}'(-1)^{(k+l-1)/2}\frac{(2k+1)(2l+1)}{(k-l)(k+l+1)}\times\frac{(k-1)!!l!!}{k!!(l-1)!!}\,\mathrm{Re}(a_ka_l^*+b_kb_l^*)+2\sum_{k=1}^{\infty}{}'\sum_{l=1}^{\infty}{}'(-1)^{(k+l)/2}\frac{(2k+1)(2l+1)}{k(k+1)l(l+1)}\times\frac{k!!l!!}{(k-1)!!(l-1)!!}\,\mathrm{Re}(a_kb_l^*)\Big], \tag{5}$$

TABLE 1. Comparison of the fractional differences $f_i=(Q_b^A-Q_b^{N_i})/Q_b^A$ between Q_b values. (See text for definitions.) Our interval-halving process was terminated when the fractional change was less than 10^{-3} in going from $N_1/2$ to N_1 and less than 10^{-6} in going from $N_2/2$ to N_2.

x	N_1	$f_1\times10^6$	N_2	$f_2\times10^9$
1	8	−29	64	− 7
2	16	−17	64	−64
3	16	−46	128	−11
4	16	− 9	128	− 1
5	16	24	128	5
10	32	41	256	10
15	64	−12	256	−41
20	64	−42	256	− 6
25	64	12	256	59
30	128	−10	512	−36
35	128	14	512	51
40	128	−27	1024	− 6
45	128	14	1024	4
50	128	14	1024	4
60	256	2	1024	8
70	256	2	1024	7
80	256	−14	1024	−48
90	256	−21	2048	4
100	256	14	2048	3

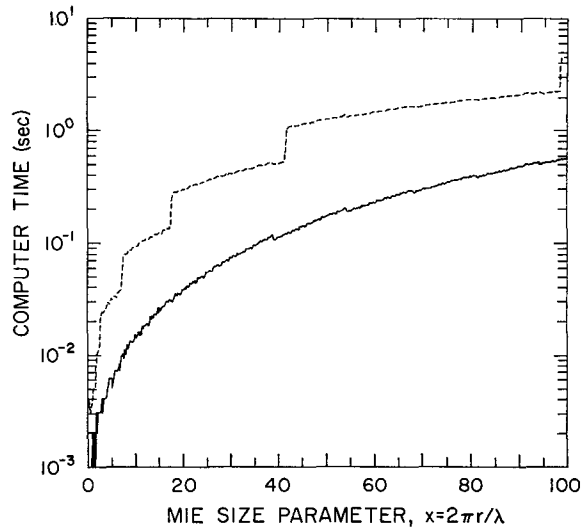

FIG. 1. Comparison of computer time required for numerical integration (dashed line) and the analytic formula (solid line) in evaluation of the backscattering efficiency Q_b.

where $\sum'$ means summation over odd integers and $\sum''$ over even integers. The double factorial $k!!$ is defined by $k!!=k[(k-2)!!]$ and $1!!=0!!=1$.

This paper verifies the analytical expression (5) by comparing it to numerical evaluations of (1), and also demonstrates its computational economy. Moreover, a number of useful applications of the analytical result are presented.

2. Comparison of numerical and analytical results

To verify the analytic formula (5) for hemispherical backscattering cross sections σ_b, we made numerical calculations using both the analytic expression (5) and the numerical integration of (1). Efficiency factors for hemispherical backscattering $Q_b=\sigma_b/\pi r^2$ were obtained at a variety of x values. Table 1 shows fractional differences $f_i=(Q_b^A-Q_b^{N_i})/Q_b^A$, where Q_b^A is a value of an efficiency factor for hemispherical backscattering obtained from (5), and $Q_b^{N_i}$ denotes a corresponding value of Q_b obtained by numerically integrating (1). The index i denotes which of two convergence criteria is used in the numerical integration, as described below.

Numerical integrations were carried out using Simpson's rule, whereby the integral

$$I=\int_{-1}^{0}f(x)dx$$

was approximated by

$$I=\frac{h}{3}[f(-1)+4f(-1+h)+2f(-1+2h)+4f(-1+3h)+2f(-1+4h)+\cdots+4f(-3h)+2f(-2h)+4f(-h)+f(0)]. \tag{6}$$

In (6), h is the width of equally spaced subintervals into which the integration interval $(-1, 0)$ was divided; the error in the approximation can be made as small as desired by dividing the integration interval into enough subintervals, i.e., by making h small enough. The computational scheme begins by dividing the interval of integration into two subintervals and evaluating the integral for those two subintervals. Then h is halved and the integral is evaluated again. The process systematically continues by doubling the number of subintervals and calculating new values of $f(x)$ at midpoints of the previous intervals; no $f(x)$ values are recomputed using this scheme. The value of the integral is calculated for each value of h and is compared with that calculated for the previous value of h. The process was terminated according to one of two convergence criteria, denoted by the index i. When the first criterion ($i=1$) was used, the process was terminated when two successive values of the fractional difference f_1 differed by less than 10^{-3} in going from $N_1/2$ to N_1 subintervals. In using the second criterion ($i=2$), f_2 differed by less than 10^{-6} in going from $N_2/2$ to N_2 subintervals.

The results (Table 1) show that when the value of the integral changes by less than one part in 10^3 ($i=1$) in going from $N/2$ intervals to N intervals, the numerical result agreed with the analytical result to within about one part in 10^5. For the case in which the integration intervals continued to be subjected to doubling procedure until subsequent values of the integral agreed to within one part in 10^6 ($i=2$), the numerical result agreed with the analytical result to within about one part in 10^8. We conclude from this behavior that the analytic formula (5) gives an exact result. With regard to numerical integrations, we point out that the 10^{-3} test for subsequent values of the integral resulted in one part in 10^5 agreement with the analytic results. However, we regard the use of less stringent convergence criteria (10^{-2}, for example) to be a hazardous procedure as it could lead to cases in which the numerical results "converge" without actually being in approximate agreement with the exact result calculated from the analytic expression (5).

Fig. 1 shows computer time as a function of Mie size parameter for numerical integration using the $i=1$ convergence criterion (dashed line) and the analytical formula (solid line). The computing times shown apply to the case with real refractive index $m=1.55$, although they were relatively independent of the refractive index used in the calculation. The stepped behavior of computer time for the numerical integration is a result of the interval doubling procedure. As we follow each step of the dashed curve to the right, we are progressively moving from the situation where the integration intervals are just about half as small as they need be for less than 0.1% uncertainty, to the situation where the integration intervals match the less than 0.1% uncertainty requirement (just before the number of intervals is doubled and a new step begins). Comparing the two curves, we note that the analytic formula is about an order of magnitude faster than the numerical integration. Of course, additional computer time savings would ensue if even smaller uncertainty factors—the 10^{-6} convergence criterion ($i=2$), for example—are employed for the test used to terminate the Simpson's rule scheme.

3. Limiting results for hemispheric backscattering

a. Small particles: Results obtained using the analytic expression

In addition to its computational advantages, the analytical result (5) is also useful for demonstrating how the hemispherical backscattering cross section behaves under various limiting conditions. For example, in the case of Rayleigh scattering by very small particles, the hemispherical backscattering cross section σ_b must be exactly one-half the total scattering cross section of the particle σ_{sc}. This result is immediately obtainable from (5), using the fact that, in the Rayleigh approximation, all Mie scattering functions but a_1 are equal to zero. We therefore have $\mathrm{Re}(a_k a_l^* + b_k b_l^*) = \mathrm{Re}(a_k b_l^*) = 0$, and from (5) we get

$$\sigma_b = \frac{3\lambda^2}{4\pi} |a_1|^2 \tag{7}$$

which is just equal to $\sigma_{sc}/2$.

In the case of small totally reflecting spheres, we have to consider the contribution from both the lowest electric wave and the magnetic wave, and we have $b_1 \neq 0$ as well as $a_1 \neq 0$. This leads to a strong backward-forward asymmetry in which the cross section for the scattering into the backward hemisphere σ_b is four times the cross section for the scattering into the forward hemisphere σ_f. In the lowest power of x the Mie scattering functions a_1 and b_1 are given by Kerker (1969):

$$a_1 = \frac{2i}{3} x^3, \tag{8a}$$

$$b_1 = -\frac{i}{3} x^3. \tag{8b}$$

For the hemispherical backscattering cross section we have from (5)

$$\sigma_b = \lambda^2/4\pi [3(|a_1|^2 + |b_1|^2) - 9/2\ \mathrm{Re}(a_1 b_1^*)] = 8x^6/3. \tag{9}$$

Since, however, the scattering cross section σ_f for scattering into the forward hemisphere is given by an expression that has the form of Eq. (5) with minus signs in front of the double sums (Chýlek, 1973),

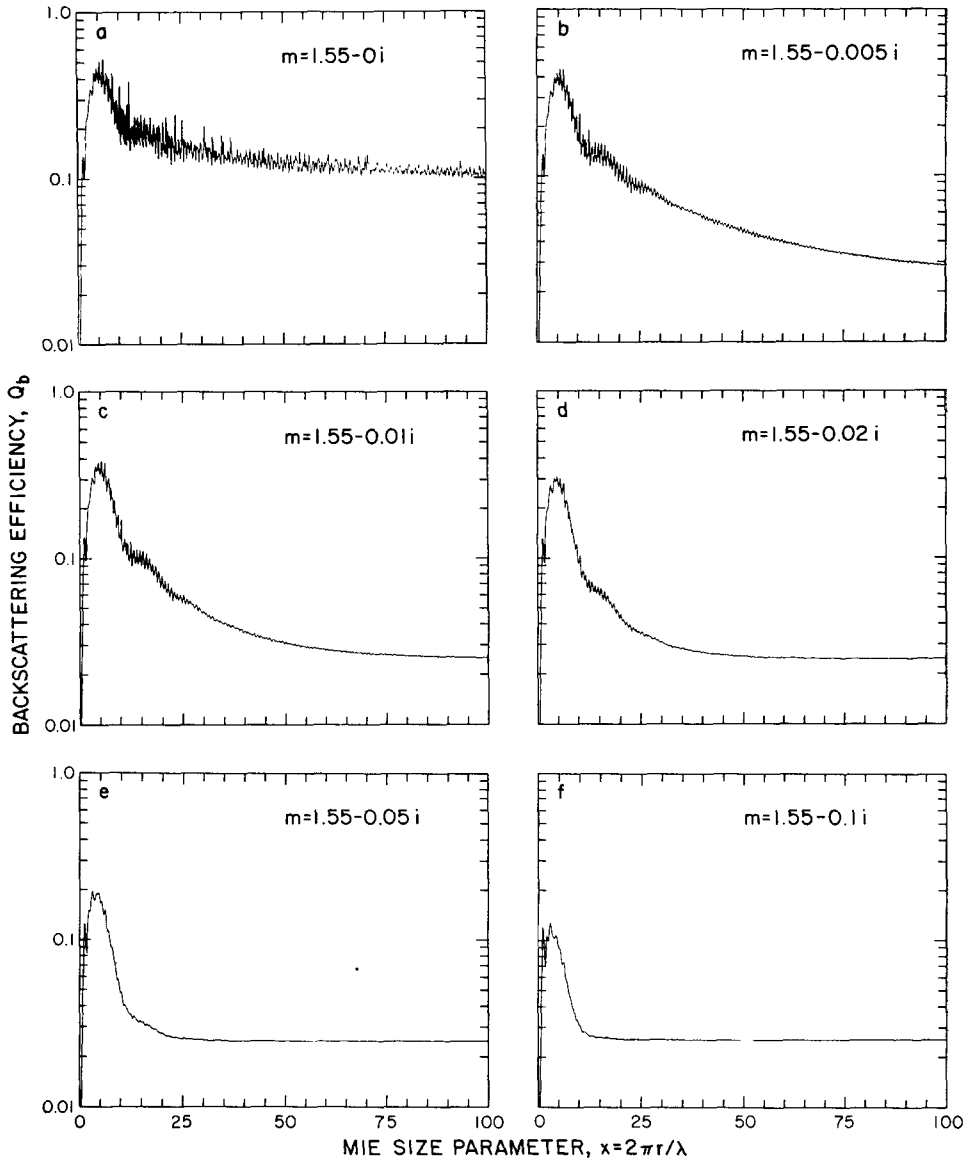

FIG. 2. The backscattering efficiency Q_b as a function of size parameter x for indicated imaginary parts n' of the complex refractive index $m=1.55-in'$.

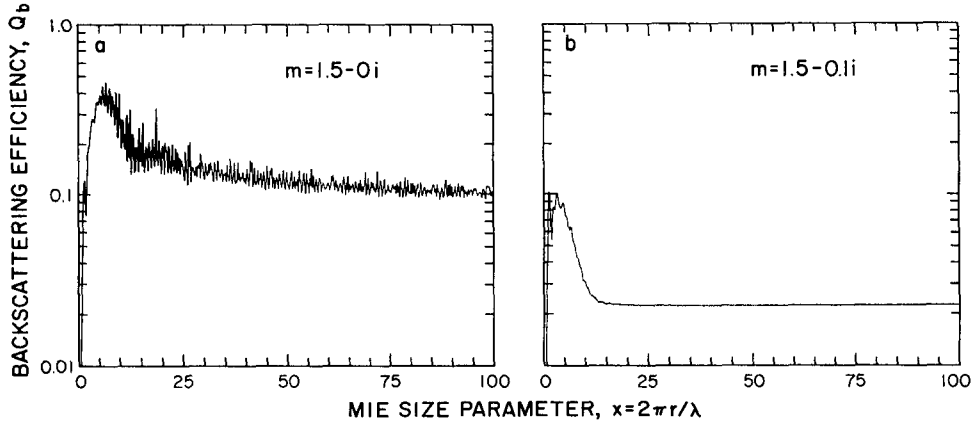

FIG. 3. The backscattering efficiency Q_b as a function of x for $m=1.50-0i$ and $m=1.50-0.1i$.

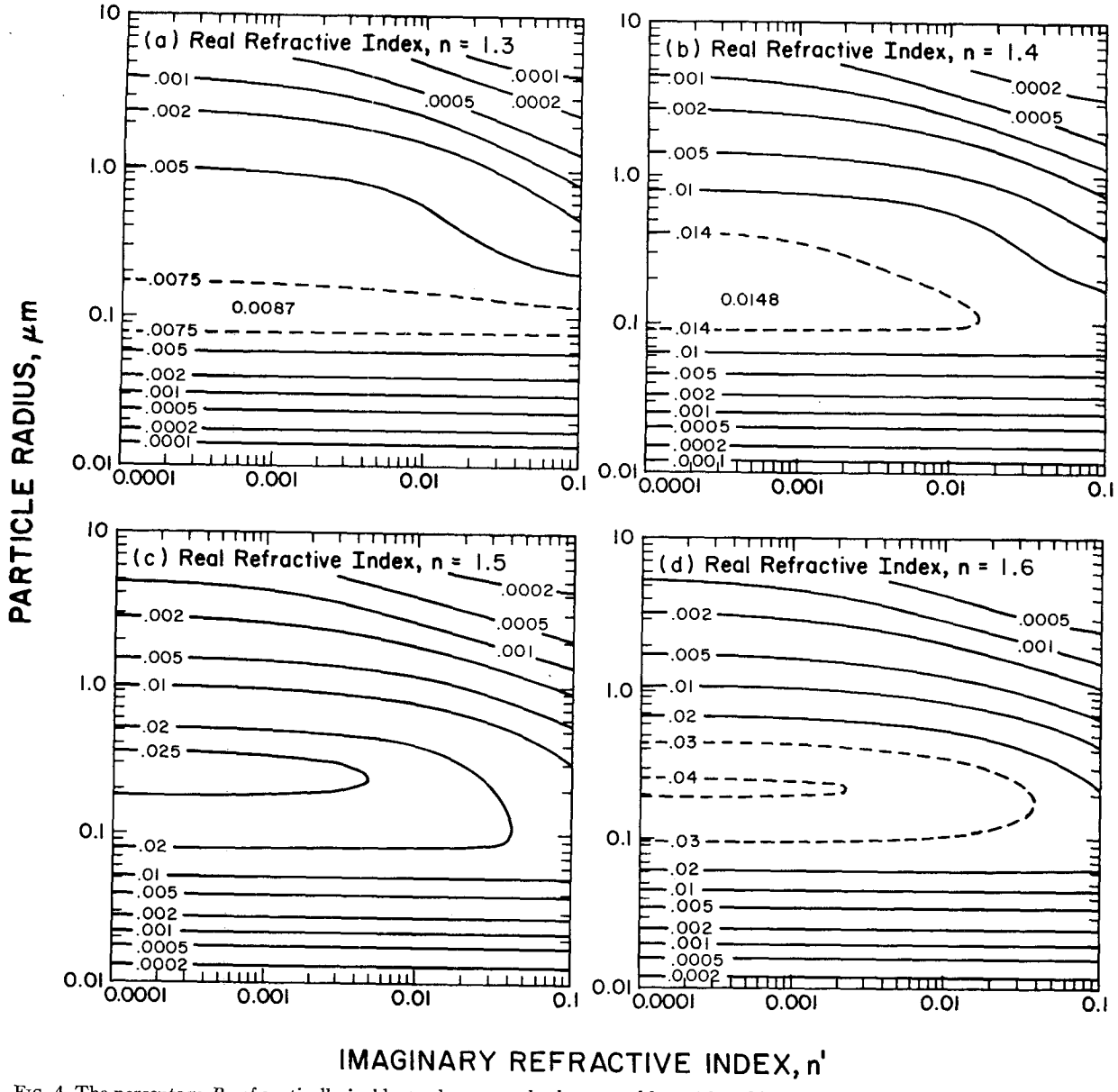

FIG. 4. The percentage P_B of vertically incident solar energy backscattered by a 1 km thick layer of spherical particles having mass concentration 1 μg m^{-3} and specific gravity 2 as a function of particle size and imaginary refractive index. Real refractive indices are (a) $n=1.3$, (b) $n=1.4$, (c) $n=1.5$, (d) $n=1.6$. To obtain results for other particle layer parameters, multiply these percentages by the appropriate layer thickness t [km] and mass concentration M [μg m^{-3}]; also, multiply results by $2/d$ to accommodate a specific gravity $d\neq 2$.

we have

$$\sigma_f=\lambda^2/4\pi[3(|a_1|^2+|b_1|^2)+9/2\ \mathrm{Re}(a_1b_1^*)]$$
$$=2x^6/3. \qquad (10)$$

Thus, small totally reflecting spheres (or small spheres with a very large imaginary part of the refractive index) can scatter up to 80% of the scattered electromagnetic radiation into the backward hemisphere.

b. Large particles: Relation to Fresnel reflection and geometrical optics

The behavior of an efficiency factor for the hemispherical backscattering Q_b for larger spheres is shown in Fig. 2. The graphs show the efficiency factor Q_b as a function of size parameter x for the six indicated values of the complex refractive index $m=n-n'i$. For non-absorbing particles with $m=1.55$ the value of Q_b decreases from $\sim$50% at $x=5$ to $\sim$10% at $x=100$. Absorbing particles have even smaller cross sections for hemispherical backscattering. With larger imaginary parts n' of the refractive index, the curves tend to approach a constant value of about $2\frac{1}{2}$% with increasing size parameter x.

The tendency to approach a constant limit with increasing x is similar to the behavior of the normal-

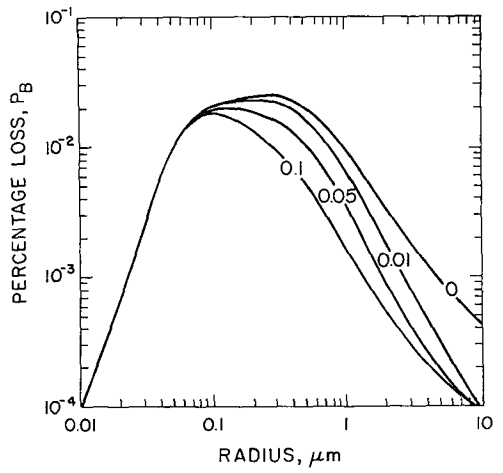

FIG. 5. The percentage P_B of vertically incident solar energy backscattered by a 1 km thick layer of spherical particles having mass concentration 1 μg m^{-3} and specific gravity 2 as a function of particle radius. Graphs refer to particles with real refractive index $n=1.5$, and the indicated imaginary refractive indices n'.

ized radar cross section which approaches a constant equal to the Fresnel reflection coefficient for normal incidence (Grams *et al.*, 1972). Similarly, we can conjecture the large x limit of the efficiency factor Q_b for the hemispherical backscattering, by considering a sphere which is very large compared to the wavelength so that geometric optics can be applied. In this case, the area-weighted reflectivities, as given by the Fresnel reflection formulas, can be used to determine the total amount of light scattered (reflected in the geometric optics limit) in all directions over the backward hemisphere. We thereby evaluate a hemispherical backscattering cross section for the geometric optics limit

$$Q_b^*=\int_0^{\pi/4}(R_{\mathrm{TE}}+R_{\mathrm{TM}})\sin\theta_i d\theta_i, \tag{11}$$

where

$$R_{\mathrm{TE}}=\left|\frac{\cos\theta_i-(m^2-\sin^2\theta_i)^{\frac{1}{2}}}{\cos\theta_i+(m^2-\sin^2\theta_i)^{\frac{1}{2}}}\right|^2, \tag{12a}$$

$$R_{\mathrm{TM}}=\left|\frac{-m^2\cos^2\theta_i+(m^2-\sin^2\theta_i)^{\frac{1}{2}}}{m^2\cos^2\theta_i+(m^2-\sin^2\theta_i)^{\frac{1}{2}}}\right|^2, \tag{12b}$$

and θ_i is the angle of incidence. We have evaluated the integral in (11) for absorbing spheres with $n=1.55$ and the same non-zero n' values in Fig. 2 ($n'=0.005$, 0.01, 0.02, 0.05, 0.1). We found that Q_b^* values calculated using the Fresnel reflection formulas and Q_b values calculated using the analytic expression at $x=200$ agreed to within 1% for all five cases. We concluded that large x values for absorbing spheres are in good agreement with values obtained from the Fresnel reflection formulas.

We also evaluated Q_b for $n=1.50$ and for two values of n' (0 and 0.1) for comparison with $n=1.55$ calculations. Results are shown in Fig. 3. The Q_b values for $m=1.50-0.1i$ are similar to those obtained in the $m=1.55-0i$ case. As would be expected from calculations using Fresnel refraction formulas, Q_b values for $m=1.50-0.1i$ approach a somewhat lower value than those obtained in the $m=1.55-0.1i$ case.

4. Applications to climate modeling

The analytic expression (5) may be utilized to obtain several results which are directly applicable to the prediction of climate change induced by aerosol pollution. For example, Fig. 4 shows the percentage P_B of incident solar radiation scattered into the backward hemisphere (i.e., back to space) by an optically thin aerosol layer consisting of mono-disperse spherical particles with specific gravity $d=2$ and mass concentration $M=1$ μg m^{-3}; the geometrical thickness of the layer is taken to be 1 km. Results are presented as contours of constant values of P_B for a range of particle radii and imaginary refractive indices for real refractive index values (a) $n=1.3$, (b) $n=1.4$, (c) $n=1.5$, (d) $n=1.6$. Thus, for example, particles characterized by an isopleth labelled 0.01 would scatter 0.01% of incident solar radiation back to space. To obtain results for layers of different thicknesses and mass concentrations, P_B values from Fig. 4 should be multiplied by the appropriate thickness t [km] and mass concentration M [μg m^{-3}]. Similarly, different specific gravities d can be accommodated by multiplying the results by $2/d$.

The results of Fig. 4 were obtained in the following manner: We assumed that the spectral distribution of the incident solar radiation followed the Plank distribution function $B(\lambda,T)$ for a blackbody of temperature $T=6000$ K. We neglected wavelenghts $\lambda<0.3$ μm as a crude approximation for the effect of ozone absorption. We then calculated by numerical integration the percentage loss

$$P_B=\frac{\displaystyle\int_{0.3\ \mu\mathrm{m}}^{\infty}N\pi r^2Q_b(\lambda,r,m)B(\lambda,T)d\lambda}{\displaystyle\int_{0.3\ \mu\mathrm{m}}^{\infty}B(\lambda,T)d\lambda}\times 100, \tag{13}$$

where N is the number of particles of radius r [μm] per unit volume. For mass concentration M, specific gravity d and particle radius r, it follows that

$$N[\mathrm{cm}^{-3}]=\frac{3}{4\pi}\frac{M}{r^3d}, \tag{14}$$

which leads to

$$P_B[\mathrm{km}^{-1}]=\frac{0.075M}{rd}\frac{\displaystyle\int_{0.3\ \mu\mathrm{m}}^{\infty}Q_B(\lambda,r,m)B(\lambda,T)d\lambda}{\displaystyle\int_{0.3\ \mu\mathrm{m}}^{\infty}B(\lambda,T)d\lambda}. \tag{15}$$

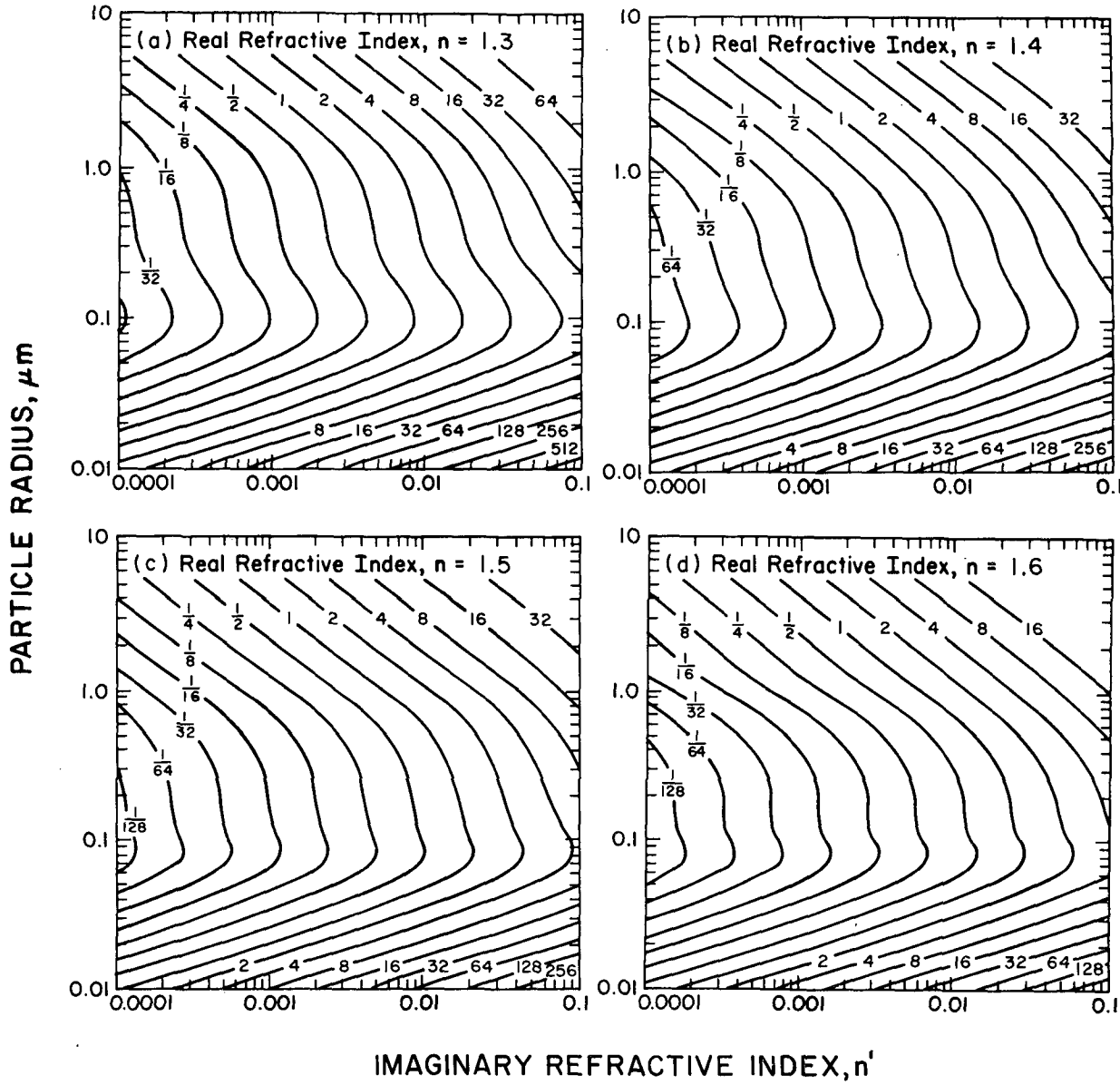

FIG. 6. The ratio ρ of particle absorption cross section to hemispherical backscattering cross section for spherical particles illuminated by solar radiation. Contours show ρ as a function of particle radius and imaginary refractive index n' for four different real refractive indices: (a) $n=1.3$, (b) $n=1.4$, (c) $n=1.5$, (d) $n=1.6$.

The analytic expression (5) may of course be integrated over specific size distributions $N(r)$ and used in (13) to obtain results for the more realistic case of a polydisperse aerosol layer. However, given the multiplicity of particle size distribution types and parameters, the contour presentation of Fig. 4 was chosen as the most compact way to indicate the dependence of hemispheric backscattering on particle size and refractive index for a fixed mass of particulate material.

The importance of the imaginary refractive index in determining hemispheric backscattering has been frequently recognized. The importance of particle size can be emphasized by replotting the results of Fig. 4c in Fig. 5 under a different format. The results show the percentage P_B of incident solar radiation backscattered by a 1 km thick layer having a fixed mass concentration (1 μg m^{-3}) for particles with a real refractive index $n=1.5$ and an indicated imaginary refractive index value n'; they clearly emphasize the fact that particles with radii between 0.1 and 0.3 μm are the most efficient hemispheric backscatterers. If the same mass of material were distributed in particles of radius less than 0.03 μm or larger than 3.0 μm, the backscattering loss would be an order of magnitude less.

As has been frequently pointed out by many climate modelers, aerosol layers may absorb radiation as well as scatter it back to space. Thus, in considering the effect of an aerosol layer on surface temperatures, the influence of aerosol layer heating must be considered. For a stratospheric aerosol layer, which has no convective contact with the surface, the above treatment describes the most important[2] and direct effect, namely the denial of solar radiation to lower layers and the earth's surface. However, for aerosol layers in convective contact with the surface, the coupled effects of absorption and backscattering must be jointly considered. Many models which have included such a joint treatment [we have cited. Atwater (1970), Mitchell (1971), Ensor *et al.* (1971) and Chýlek and Coakley (1974) as examples] have shown that a critical parameter in determining whether an aerosol layer will heat or cool the surface is the ratio ρ of absorption to hemispheric backscattering. The same ratio ρ also determines the net heating effect of any aerosol layer in the optically thin limit (regardless of its surface contact) on the earth-atmosphere system. Therefore, as an aid in implementing such model results, we present Fig. 6 (similar to Fig. 4) giving results for the ratio ρ of absorption to hemispheric backscattering for various monodisperse aerosol layers. We obtained the results presented in Fig. 6 by numerical integrations of the ratio

$$\rho=\frac{P_A}{P_B}=\frac{\int_{0.3\ \mu m}^{\infty} Q_A(\lambda,v,m)B(\lambda,T)d\lambda}{\int_{0.3\ \mu m}^{\infty} Q_B(\lambda,v,m)B(\lambda,T)d\lambda}, \qquad (16)$$

where P_A is the percentage of incident solar radiation absorbed by the particles and Q_A the particle absorption coefficient. The percentage P_A of solar radiation absorbed by the particles can, of course, be determined by multiplying the P_B and ρ results obtained from Figs. 4 and 6.

[2] This discussion neglects any effects on stratospheric dynamics which may result from local aerosol heating.

5. Conclusions

The analytic expression (5) for the hemispherical backscattering cross section gives correct results, and it also saves computer time. Furthermore, the analytic expression provides better insight as to how the hemispherical backscattering cross section behaves under various approximations or limiting conditions. In addition, we have conjectured that the large x limit of Q_b is given by the expression (11). Finally, we utilized the analytic expression (5) to obtain the resulting Figs. 4–6, which may be useful for a variety of climatic modeling applications.

Acknowledgments. The first author was supported in part by the Atmospheric Sciences Section of the National Science Foundation under Grant A041786, and in part by a State University of New York Grant-in-Aid.

REFERENCES

Atwater, M. A., 1970: Planetary albedo changes due to aerosols. *Science*, **170**, 64–66.

Chýlek, P., 1973: Mie scattering into the backward hemisphere. *J. Opt. Soc. Amer.*, **63**, 1467–1471.

——, and J. A. Coakley, Jr., 1974: Aerosols and climate. *Science*, **183**, 75–77.

Ensor, D. S., W. M. Porch, M. J. Pilat and R. J. Charlson, 1971: Influence of atmospheric aerosol on albedo. *J. Appl. Meteor.*, **10**, 1303–1306.

Grams, G. W., I. H. Blifford, Jr., B. G. Schuster and J. J. DeLuisi, 1972: Complex index of refraction of airborne flash determined by laser radar and collections of particles at 13 km. *J. Atmos. Sci.*, **29**, 900–905.

Kerker, M., 1969: *The Scattering of Light and Other Electromagnetic Radiation*. Academic Press, p. 90.

Mitchell, J. M. Jr., 1971: The effect of atmospheric aerosols on climate with special reference to temperature near the earth's surface. *J. Appl. Meteor.*, **10**, 703–714.